Slowdown and Recovery of the Atlantic Meridional Overturning Circulation and a Persistent North Atlantic Warming Hole Induced by Arctic Sea Ice Decline

Brady Ferster, Amélie Simon, Alexey V. Fedorov, Juliette Mignot, Éric Guilyardi

AGU ADVANCING EARTH AND SPACE SCIENCE

Geophysical Research Letters®

RESEARCH LETTER
10.1029/2022GL097967

Key Points:

- Atlantic meridional overturning circulation (AMOC) response involves compensation between changes in eastern (decline) and western (increase) subpolar North Atlantic deep convection
- Reduced sea ice results in southeastward expansion of the North Atlantic subpolar gyre and a negative North Atlantic Oscillation-like pattern
- A North Atlantic warming hole develops independently of AMOC modulation

Supporting Information:

Supporting Information may be found in the online version of this article.

Correspondence to:

B. S. Ferster,
brady.ferster@locean.ipsl.fr

Citation:

Ferster, B. S., Simon, A., Fedorov, A., Mignot, J., & Guilyardi, E. (2022). Slowdown and recovery of the Atlantic meridional overturning circulation and a persistent North Atlantic warming hole induced by Arctic sea ice decline. *Geophysical Research Letters*, *49*, e2022GL097967. https://doi.org/10.1029/2022GL097967

Received 11 FEB 2022
Accepted 17 AUG 2022

Slowdown and Recovery of the Atlantic Meridional Overturning Circulation and a Persistent North Atlantic Warming Hole Induced by Arctic Sea Ice Decline

Brady S. Ferster[1], Amélie Simon[1,2], Alexey Fedorov[1,3], Juliette Mignot[1], and Eric Guilyardi[1,4]

[1]LOCEAN-IPSL (Sorbonne Université, CNRS, IRD, MNHN), Paris, France, [2]Faculdade de Ciências, Instituto Dom Luiz (IDL), Universidade de Lisboa, Lisboa, Portugal, [3]Department of Earth and Planetary Sciences, Yale University, New Haven, CT, USA, [4]NCAS-Climate, University of Reading, Reading, UK

Abstract We investigate the impact of Arctic sea ice loss on the Atlantic meridional overturning circulation (AMOC) and North Atlantic climate in a coupled general circulation model (IPSL-CM5A2) perturbation experiment, wherein Arctic sea ice is reduced until reaching an equilibrium of an ice-free summer. After several decades we observe AMOC weakening caused by reduced dense water formation in the Iceland basin due to the warming of surface waters, and later compensated by intensification of dense water formation in the Western Subpolar North Atlantic. Consequently, AMOC slightly weakens in deep, dense waters but recovers through shallower, less dense waters overturning. In parallel, wind-driven intensification and southeastward expansion of the subpolar gyre cause a depth-extended cold anomaly ~2°C around 50°N that resembles the North Atlantic "warming hole." We conclude that compensating dense water formations drive AMOC changes following sea ice retreat and that a warming hole can develop independently of the AMOC modulation.

Plain Language Summary To investigate the impact of Arctic sea ice loss due to anthropogenic warming on climate, we have designed experiments using an atmosphere-ocean coupled general circulation model reducing the Arctic sea ice albedo in order to match future sea ice reduction. The induced changes in the summer Arctic sea ice reflect projections of an ice-free summer Arctic. To examine the impact of a reduced Arctic sea ice state we investigate the Atlantic meridional overturning circulation (AMOC), due to the long timescales involved in ocean circulation. In response to Arctic sea ice decline, our results indicate that the decline in dense waters in the eastern subpolar region are partly compensated by an increase in the western subpolar North Atlantic, resulting in a modest decline and then recovery of AMOC. Our results further reveal that an anomalous warming hole feature forms as a result of the changes in atmospheric circulation and ocean gyres, independent of the strength of AMOC.

1. Introduction

Beyond its role in regulating the earth global albedo, the Arctic sea ice plays an important role in regulating atmosphere-ocean fluxes: exposed ocean surface allows for an enhanced transfer of momentum, energy, and mass, yielding the ocean particularly vulnerable to a warming climate inducing sea-ice melting. Arctic sea ice extent has been decreasing by 13% per decade between 1979 and 2018 (Meredith et al., 2019). A majority of Climate Model Intercomparison Project (CMIP) projections estimate an ice-free summer Arctic by the year 2050, but the its exact timing varies by decades depending on models' sensitivity and internal variability (Notz and SIMIP Community, 2020).

Despite taking place over a relatively small percentage of the global oceans, the impacts of sea ice decline and an ice-free Northern Hemisphere pole extend far beyond the Arctic and subarctic regions (e.g., Deser et al., 2015). For example, he observed late autumn Arctic sea ice loss has been shown to be associated with a negative North Atlantic Oscillation (NAO) winter pattern (Caian et al., 2018; García-Serrano et al., 2015; Simon et al., 2020) in observations. Yet, outside of the Arctic and North Atlantic, there is ongoing debate on the significance of the impact of sea ice decline (Cohen et al., 2014; Overland and Wang, 2013). The discrepancy in models was recently associated with an underestimated eddy feedback (Smith et al., 2022). Indeed, given the lack of spatio-temporal observations in the Arctic and in the ocean overturning circulation, coupled atmosphere-ocean general circulation (GCM) models are typically used to analyze atmospheric and oceanic responses to Arctic sea ice decline.

To isolate the impact of retreating Arctic sea ice from the more general climate response to anthropogenic warming, some modeling groups modify sea-ice properties, such as emissivity, albedo, thermal conductivity (Blackport and Kushner, 2016; Cvijanovic et al., 2017; Sévellec et al., 2017; Simon et al., 2021), while others modify heat flux onto the sea-ice (Deser et al., 2015; Oudar et al., 2017; Tomas et al., 2016). Both approaches aim at mimicking the observed sea ice melting. Similar to observations, these experiments show a negative NAO-like response in the winter to sea ice decline (Blackport and Kushner, 2016; Deser et al., 2015; Oudar et al., 2017; Screen et al., 2018; Suo et al., 2017). Due to the low frequency and long-timescales of ocean circulation (i.e., multi-decadal to centennial frequency), the long-term climate impacts of Arctic sea ice decline are often analyzed through the response of the North Atlantic Oscillation (AMOC) (Zhang, 2015). Two particular responses to sea ice decline emerge in modeling studies: those that exhibit a weak decline in AMOC followed by a recovery (Blackport and Kushner, 2016; Tomas et al., 2016) and those that show the transition to a much weaker AMOC state (Liu et al., 2019; Liu and Fedorov, 2019; Oudar et al., 2017; Sévellec et al., 2017; Sun et al., 2018; Suo et al., 2017). In fact, even different configurations of the same model can show these different responses (Li et al., 2021; Li and Fedorov, 2021). More recently, Liu and Fedorov (2022) identified the latter type of response in Arctic sea ice/AMOC multi-decadal variability in CMIP5 and CMIP6 models.

The objective of this study is to revisit the results of previous experiments imposing Arctic sea ice decline. The transient to equilibrium response of the climate to Arctic sea ice loss is examined with a coupled model from the Institut Pierre-Simon Laplace, with emphasis on drivers and mechanisms of AMOC and middle-to-high latitude North Atlantic climate responses. We aim to identify the mechanism explaining the AMOC response within our experiment, knowing that it can be model-dependent based on the North Atlantic deep-convective sites and on the initial state of the sea ice extent.

2. Model Set-Up

2.1. Model Description

The IPSL-CM5A2 (Sepulchre et al., 2020) is very similar to the IPSL-CM5A-LR version of the model used for CMIP5 (Dufresne et al., 2013), the main difference relying on computation optimization. It uses the ocean model NEMOv3.6 (Madec and the NEMO Team, 2016) on the ORCA2 grid with 182×149 cells. There are 31 non-uniform vertical levels, with increasing cell thickness with depth. The atmospheric model is LMDZ version 5A (Hourdin et al., 2013) and the grid is composed of 95×95 cells, with 39 vertical levels from the surface up to 4 Pa. The IPSL-CM5A2 has typical biases from low resolution models. For example, the Gulf Stream and North Atlantic current are too zonal and AMOC is probably underestimated, resulting in a cold bias in the North Atlantic. In the control, the maximum overturning streamfunction occurs at ~40°N, with maximum intensity of 10.5 ± 0.5 Sv as computed in z-coordinates (depth) and 5.4 ± 0.6 Sv in density coordinates (~45°N). Additionally, the seasonal minimum and maximum Arctic sea ice area (SIA) are overestimated, although improved in IPSL-CM5A2 compared to IPSL-CM5A-LR (Sepulchre et al., 2020; Simon et al., 2021). Too much sea ice in the Labrador and Irminger Seas is thought to reduce deep convection in the region and relate to the weak AMOC in the model. In Heuzé (2017), the main convective region of IPSl-CM5A-LR (as is CM5A2) is shown to be in the Western Subpolar North Atlantic (WSNA) rather than the Labrador Sea region, as the sea ice extent prevents deep convection in the Labrador Sea during winter months (Figure S1a in Supporting Information S1).

2.2. Experiments and Methodology

The experimental procedure applied here is similar to the several previous studies investigating the effects of Arctic sea ice reduction with coupled models (i.e., Blackport and Kushner, 2016; Oudar et al., 2017; Sévellec et al., 2017; Liu et al., 2019) and follows specifically Simon et al., 2021: Starting from present-day control simulations (PdControl), in which external forcings are kept constant at the level of the year 2000, it consists in artificially reducing the sea ice and snow cover albedo by −22.5%. A 14-member ensemble of 200 years-long simulations is referred to as ALB. In practice, this ensemble includes 9 members (ALB1) and 5 members (ALB2) launched respectively from two different restart points of the PdControl. ALB1 members restart from a state of low AMOC and enhanced SIA. ALB2 are restarted from a high AMOC and Arctic low sea ice background state. The 9- and 5-member ensemble of control simulations (CTRL1 and CTRL2), with same start dates and duration as the ALB1 and ALB2 ensembles is also generated, using the default albedo parameters. All anomalies are

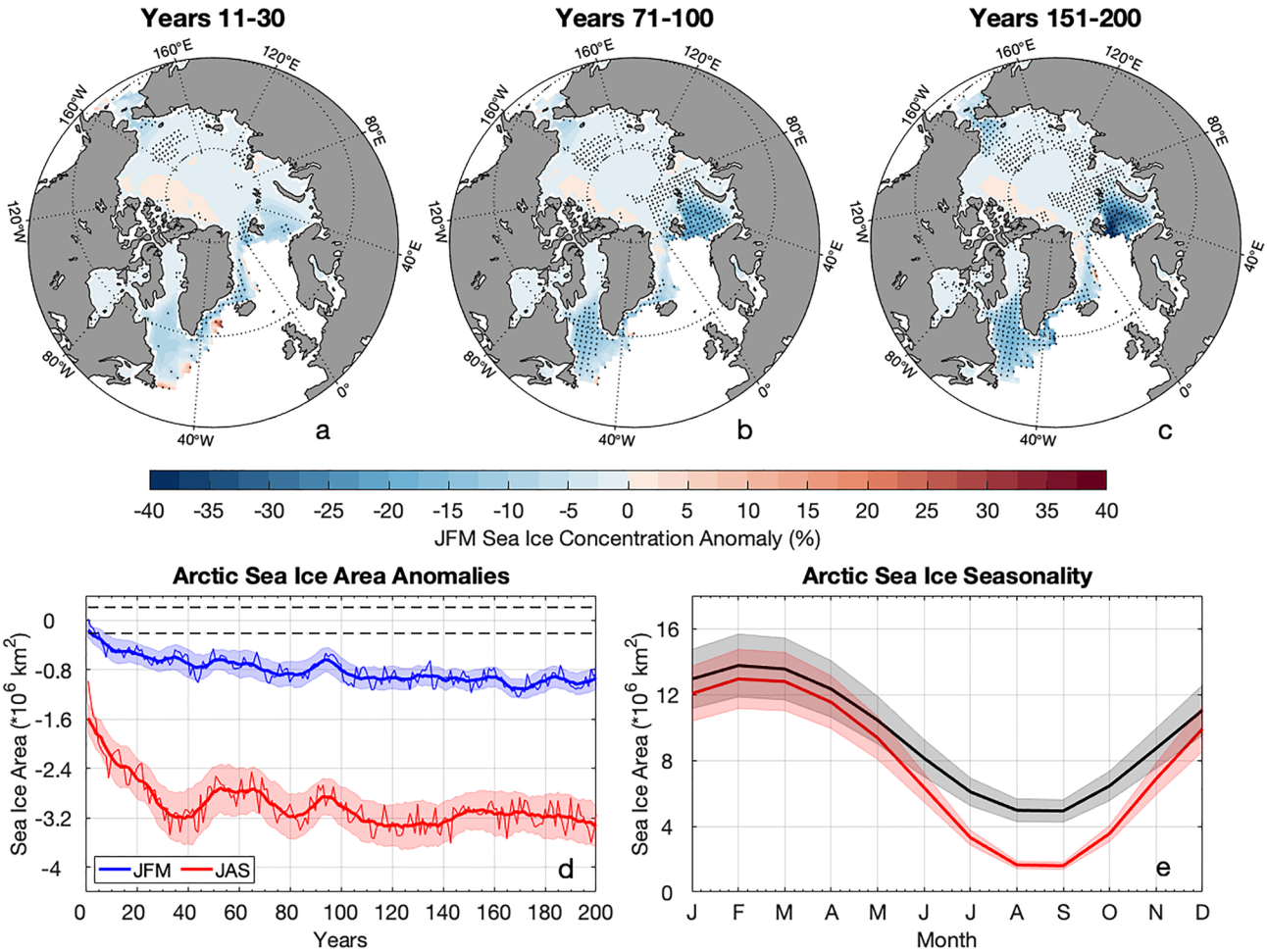

Figure 1. Ensemble mean of winter (JFM) sea ice anomalies for years (a) 11–30, (b) 71–100, and (c) 151–200 for the sea-ice perturbation experiment. Values with hatching are significant at a 95% confidence level. Induced changes in the total (d) Arctic sea ice area for winter (JFM, blue) and summer (JAS, red) and the (e) seasonality of the Arctic sea ice extent, taken for years 151–200 of the experiment. Thin and thick red lines in (c) indicate ensemble-mean and its 11-year running-mean, respectively; shading indicates ensemble spread to the 95% confidence threshold. For reference, the winter (summer) time-mean control sea ice area is $13.3 \pm 0.4 \times 10^6$ km^2 ($5.3 \pm 0.5 \times 10^6$ km^2). Summer (JAS) sea ice spatial anomalies are shown in Figure S1 in Supporting Information S1.

computed for ALB1 and ALB2 separately respectively to the CTRL1 and CTRL2 ensemble mean. This allows eliminating potential model drift and to identify the robust responses of the climate to Arctic sea ice decline. The 14-member ensemble from PdControl is named Control hereafter.

The results are then presented as a 14-member anomalous response to sea ice decline. We analyze three periods: the fast transient period from year 11–30 years, the slow transient period from years 71–100, and the quasi-equilibrium period from years 151–200 (See Figures 1 and 2). To examine the ocean surface response to the anomalous buoyancy forcing induced by sea ice melting, a water mass transformation (WMT) analysis (Speer and Tziperman, 1992; Walin, 1982) is performed. This analysis allows calculating surface dense-water formation rates (DWF) from the convergence or divergence of mass in the density space (Sv) and identifying the dominant forcing (heat, freshwater, momentum flux) for the formation of dense water in each convective region. The convective regions of the subpolar North Atlantic are broken into three basins, defined by modeled bathymetry, March mixed layer depth (MLD) variability, and sea ice extent, extending to 45°N. The regions are defined as the WSNA, Iceland Basin, and Nordic Seas. Broadly defined, the WSNA mask includes the Irminger Sea, Western Subpolar region and the Labrador Sea. DWF classifications for each region are based on the approximate maximum of densest waters of WMT in the Control.

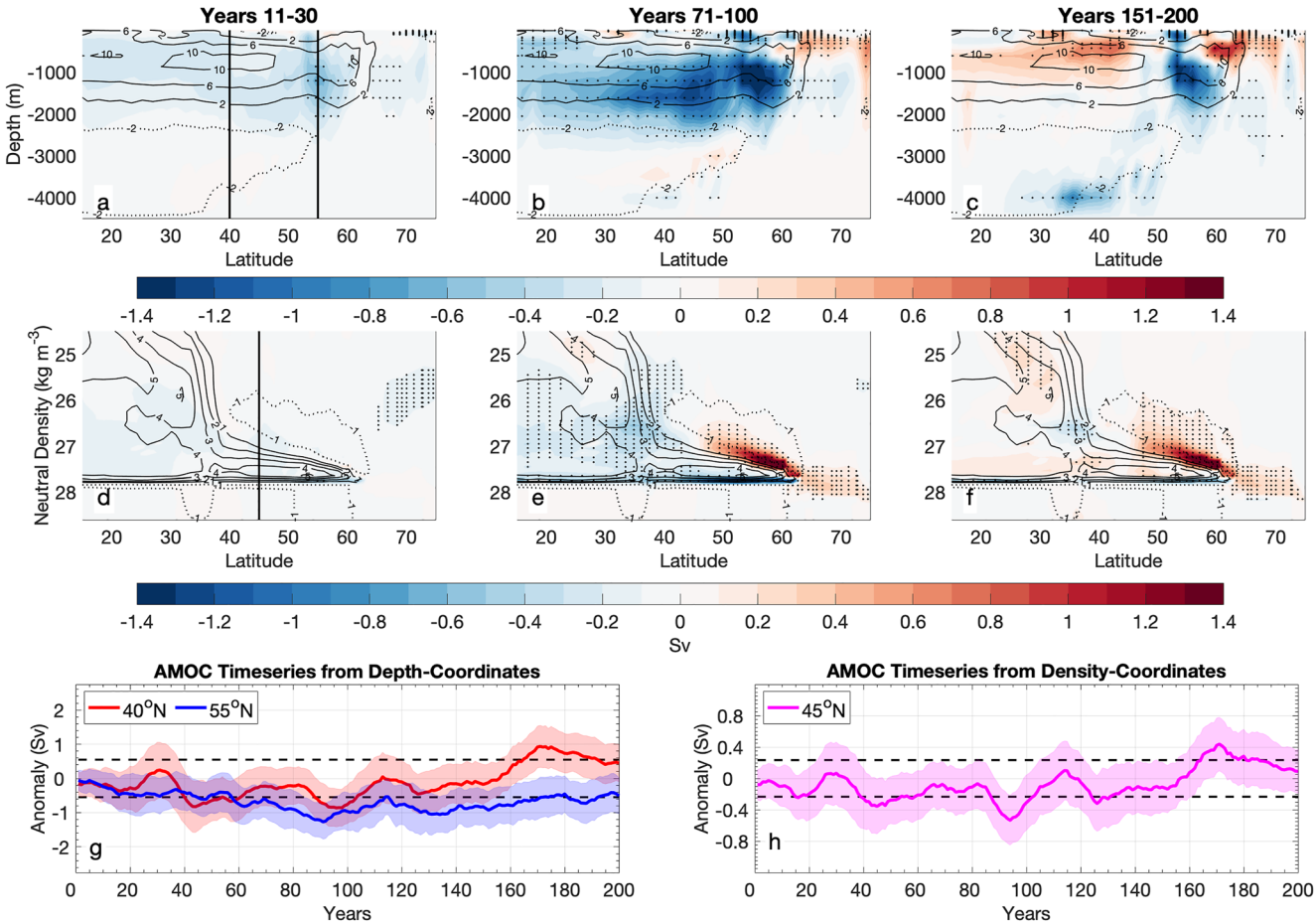

Figure 2. (a–c) Atlantic meridional overturning streamfunction in depth-coordinates for the control simulation (Sv, black contours) and its anomalies in the sea-ice perturbation experiments (color shading) for the same time intervals. (d–f) Atlantic meridional overturning streamfunction binned across neutral density coordinates (binned by 0.1 kg m^{-3}) in the control simulation (Sv, black contours) and its anomalies in the sea-ice perturbation experiments (color shading). Values with hatching are significant at a 95% confidence level. Timeseries of anomalous maximum AMOC (Sv) at (g) 40°N and 55°N from depth coordinates, similar to Simon et al. (2021), and (f) 45°N from density coordinates with an 11-year moving mean applied. The dashed black lines represent the 95% confidence interval of the control; shading indicates ensemble spread. The vertical black lines in (a,d) mark 40°N, 45°N, and 55°N—the latitudes used to evaluate AMOC strength in (g, h). The correlation of AMOC in depth and density space both at 40°N is ∼0.90 and ∼0.50 at 55°N in the control.

3. Results

3.1. The AMOC Response

The response of Arctic summer sea ice in the perturbation experiments occurs on relatively fast timescales. The summer (JAS) Arctic SIA decreases by $-3.7 \pm 0.2 \times 10^{12}$ m^2, corresponding to ∼33.5% decrease within the first 10 years of the experiment, compared to a ∼2.1% decline in winter (JFM). Although the experiment aims to reduce the Arctic summer sea ice extent, we focus on the winter sea ice changes due to the importance to ocean and atmosphere circulation. During the subsequent initial (Figure 1a, years 11–30) and slow transient phases (Figure 1b, years 71–100), a significant retreat of the winter sea ice extent occurs throughout the Irminger and Nordic Sea regions, that have too extensive sea ice cover in CM5A2 control state (Figures S1a–S1b in Supporting Information S1). The largest decline of sea ice concentration (Figure 1c) in the quasi-equilibrium stage occurs in the Barents Sea (>35% reduction) and the Labrador Sea (20%–30% reduction). The latter nevertheless remains largely covered (Figure S1c in Supporting Information S1). The Arctic SIA reaches an approximate stable response by year 60 of the experiment (Figure 1d), and is largely driven through the decline in summer sea ice (Figures 1d and 1e). These seasonal Arctic responses to changing surface albedo are consistent with several other modeling studies (i.e., Blackport and Kushner, 2016; Oudar et al., 2017; Sévellec et al., 2017; Liu et al., 2019).

In the initial transient period (years 11–30), there is a weakening of ∼−0.5 Sv of the overturning circulation in depth-coordinates (Figure 2a) occurring at the approximate maxima in the overturning cell (40°N). Throughout the slow transient period (years 71–100), the overturning cell further weakens by additional ∼1 Sv between 30° and 60°N, mostly below 1,000 m depth (Figure 2b), and the overturning shallows. Around both 40°N (mid-latitudes) and 55°N (subpolar region), the largest anomalous decline occurs between years 71 and 100. The largest response occurs between 50° and 55°N, where it reaches nearly −1.5 Sv, corresponding to a 15% reduction. Nevertheless, in the regions 30°–40°N and 60°–70°N a positive overturning streamfunction anomaly of ∼0.5 Sv develops within the top 500 m. The last 50 years of the experiment display generally positive overturning anomalies of ∼0.6 Sv between 30° and 50°N (surface-1000 m), while negative anomalies persist between 50° and 60°N (Figure 2c). A similar comparison in density-coordinates (Figures 1d–1f) indicates a shift of the overturning cell to less dense waters in the North Atlantic subtropics and subpolar (north of ∼45°N) regions. Overall, the AMOC shallows and weakens at depth, but subsequently recovers its strength through shallower, less dense overturning. The ALB timeseries of AMOC at 40°N (Figure 2g) does not exceed the mean state of the control between years 151–200 (11.3 ± 0.5 Sv relative to the 10.5 ± 0.7 control time mean and 95% confidence interval). AMOC at 55°N (Figure 2g) exhibits a weaker state where the ALB mean is 7.7 ± 0.5 Sv relative to the control mean of 8.3 ± 0.5 Sv for years 151–200. However, meridional overturning circulation evaluated in z-coordinates alone can be misleading at high latitudes (Kwon and Frankignoul, 2014). Consistently, correlations of depth- and density-coordinates at the same latitude for AMOC drop from 0.90 at 40°N to 0.50 at 50°N in the Control ensemble. The timeseries of AMOC in density coordinates at 45°N (approximate maximum, Figure 2f) in ALB does not exceed the control (4.3 ± 0.3 Sv in ALB, 4.1 ± 0.3 in Control). The timeseries of AMOC remain within the variability of the control between years 151–200, using a combination of depth-coordinates south of the North Atlantic subpolar and density-coordinates within the approximate subpolar region (for as explained in Kwon and Frankignoul (2014)).

In the transient periods, there is a deepening of ∼200 m of the winter MLD (Figures 3a–3d) in the WSNA, which represents a significant response of the convective regions. The quasi-equilibrium state displays a deeper mixed layer, by nearly 300 m, in the WSNA, and a shallower mixed layer in the Iceland basin by −50 to −250 m depth with respect to the control conditions (Figure 3d). In the top 500 m of the North Atlantic, there are temperature (Figures S2a–S2c in Supporting Information S1) and salinity (Figures S2d–S2f in Supporting Information S1) anomalies, driving an anomalous zonal density (Figures S2g–S2i in Supporting Information S1) gradient across the WSNA and Eastern Subpolar North Atlantic.

A WMT analysis is used to quantify the importance of buoyancy driven anomalies in the formation of surface waters. DWF at densities greater than $\sigma = 27.65$ kg m^{-3} (threshold identified Figure S3 in Supporting Information S1) in the WSNA significantly increases throughout the experiment, exceeding the envelope of the control within the first decade of the experiment. This means that as Arctic sea ice declines, there is a net positive anomalous formation of dense water in the WSNA of 4.3 ± 1.2 Sv over the 200 years (Figures 3e, 6.1 ± 2.1 Sv for years 151–200). In contrast, the DWF in the Iceland basin (threshold of 27.60 kg m^{-3}) decreases by −5.9 ± 1.0 Sv (Figure 3e, −5.6 ± 1.8 Sv for years 151–200). The Nordic Seas WMT remains within the range of the control, but increases by 1.8 ± 0.6 Sv between years 71–170, before eventually returning to its initial value for the last 30 years. The quasi-equilibrium response to Arctic sea ice decline thus results from the compensation between an increase of DWF in the WSNA and a decrease in the Iceland basin (Figure 3e). The sum of the convective regions DWF intensities displays similar variability to $AMOC_{55N}$ from density-coordinates and to Subpolar Gyre (SPG) intensity with correlations of 0.72 and 0.58 respectively at lag-zero.

The lag-lead correlations between the DWF and the MLD, AMOC, and the SPG intensity (Figure S4 in Supporting Information S1) indicate that the WSNA is significantly positively correlated with the MLD and SPG_i at zero-lag and leads AMOC by 8 years at multiple latitudes (Figure S4a in Supporting Information S1), similar to the lag of Irminger Sea variability on AMOC from Menary et al. (2020) and Ortega et al. (2021) in other versions of the same model. On the other hand, the MLD in the Iceland basin leads DWF by 1 year and the DWF leads AMOC by ∼7 years at multiple latitudes (Figure S4b in Supporting Information S1). Moreover, DWF from the WSNA and the Iceland Basin are significantly correlated with the overturning cells in both z- and density-coordinates (Figure S5 in Supporting Information S1). The DWF from the WSNA region is positively correlated to enhanced North Atlantic overturning for waters shallower (Figure S5a in Supporting Information S1) and less dense (Figure S5b in Supporting Information S1) than the maximum, while the Iceland Basin is related to changes of AMOC

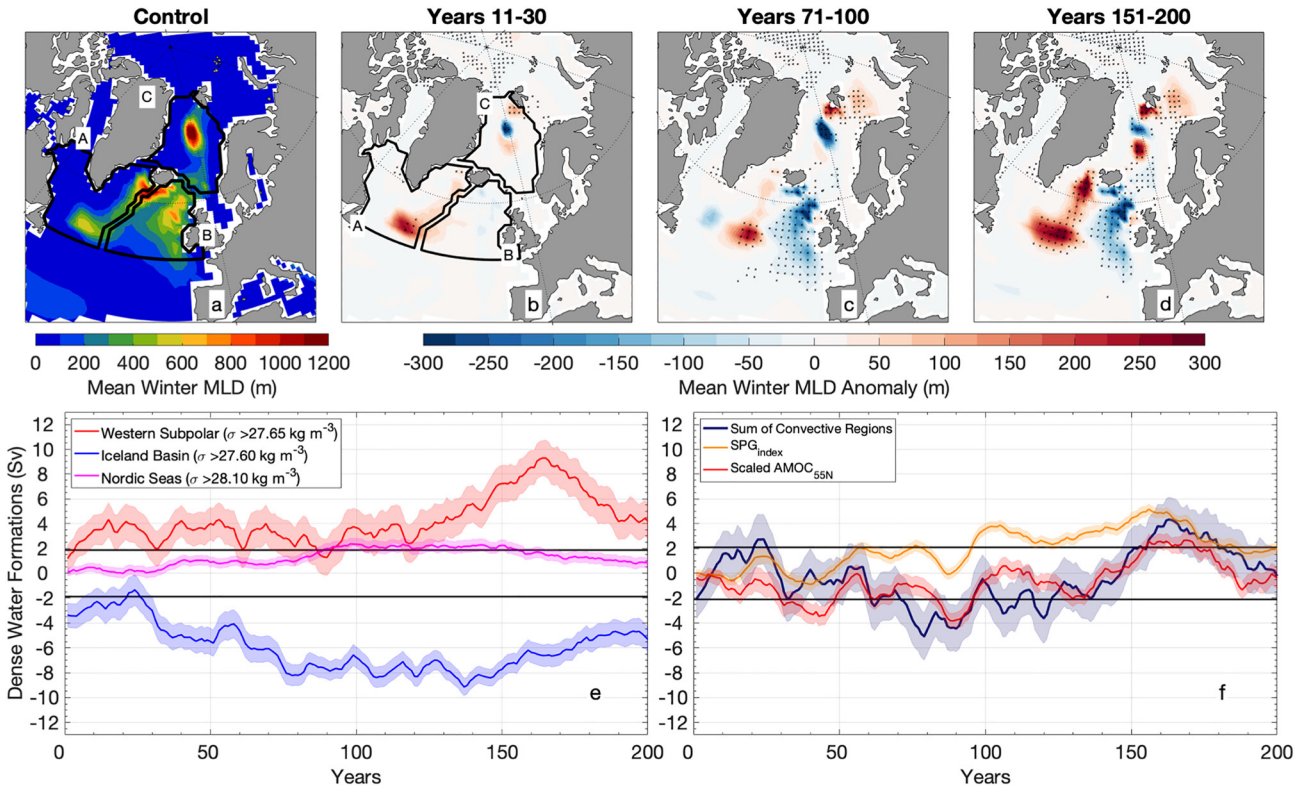

Figure 3. Mean winter (JFM) mixed layer depth (MLD) in (a) the control and (b-d) ensemble-mean anomalies in the sea-ice perturbation experiment for the same time intervals as in Figures 1 and 2. Three convective ocean basins are defined in (a) as the Labrador and Irminger Seas (a), Iceland basin (b), and Nordic Seas (c). (e-f) Ensemble-mean anomalous dense water formation rates in the perturbation experiment from a surface water mass transformation analysis; shading represents ensemble spread and an 11-year moving mean applied. Horizontal gray lines in (e-f) indicate the 95% confidence interval of the total dense water formation of the control. The entire North Atlantic convective region is represented in (f) as the sum of regions in (e). Note the large degree of compensation between changes in the (a) Labrador and Irminger Seas and the (b) Iceland Basin, which leads to AMOC decline followed by recovery. For comparison of the convective basins, the Subpolar Gyre index (SPG_{index}, absolute value of the minimum barotropic streamfunction) and a scaled $AMOC_{55N}$ index ($AMOC_{55N}$ timeseries from Figure 2h multiplied by 10) with an 11-year moving mean applied. At lag-zero, the $AMOC_{55N}$ (SPG_{index}) is correlated with the sum of the dense-water formation rates (DWF) at 0.72 (0.58), both significant at the 95% confidence level. The AMOC timeseries used is taken from density-coordinates.

between 1000 and 2500 m depths (Figure S5c in Supporting Information S1) and density-overturning in the North Atlantic subtropics and subpolar. This suggests that the Iceland Basin region DWF changes could be behind the AMOC weakening at deep, dense levels, while the WSNA region is more linked to the near-surface changes of AMOC. To conclude, the NAWS and Iceland Basin regions act to compensate for the overturning cell in this model and act to stabilize the AMOC to reduced Arctic sea ice.

3.2. Changes to the North Atlantic Climate and the Warming Hole

In parallel with changes in the North Atlantic Ocean, the imposed sea ice decline affects the North Atlantic atmospheric circulation, that can modify oceanic horizontal ocean circulation. Specifically, a winter (JFM) negative NAO-like pattern in sea level pressure (SLP) develops across the North Atlantic after year 71 (Figures S6a–S6d in Supporting Information S1), associated with a narrowing of the zonally-averaged Northern Hemisphere westerlies (Figures S6e–S6h in Supporting Information S1). Zonal winds are also enhanced in the subtropics (trades) and over the Iceland basin (westerlies) and decreased over the subpolar North Atlantic (Figures S6i–S6l in Supporting Information S1). This SLP_{NAO}-like pattern is not significant during the initial transient phase, which differs from the results of Simon et al., 2021. This suggests that the result may depend on the initial background climate state or that internal variability is high, meaning a large sample size is needed to detect the signal. We do nevertheless detect a depression over the Arctic and North Atlantic in the initial response (Figures S6b in Supporting Information S1). Furthermore, the Control simulations show that the NAO (Figures S7a in Supporting Information S1) is very similar to the anomalous SLP pattern associated with SIA intensification

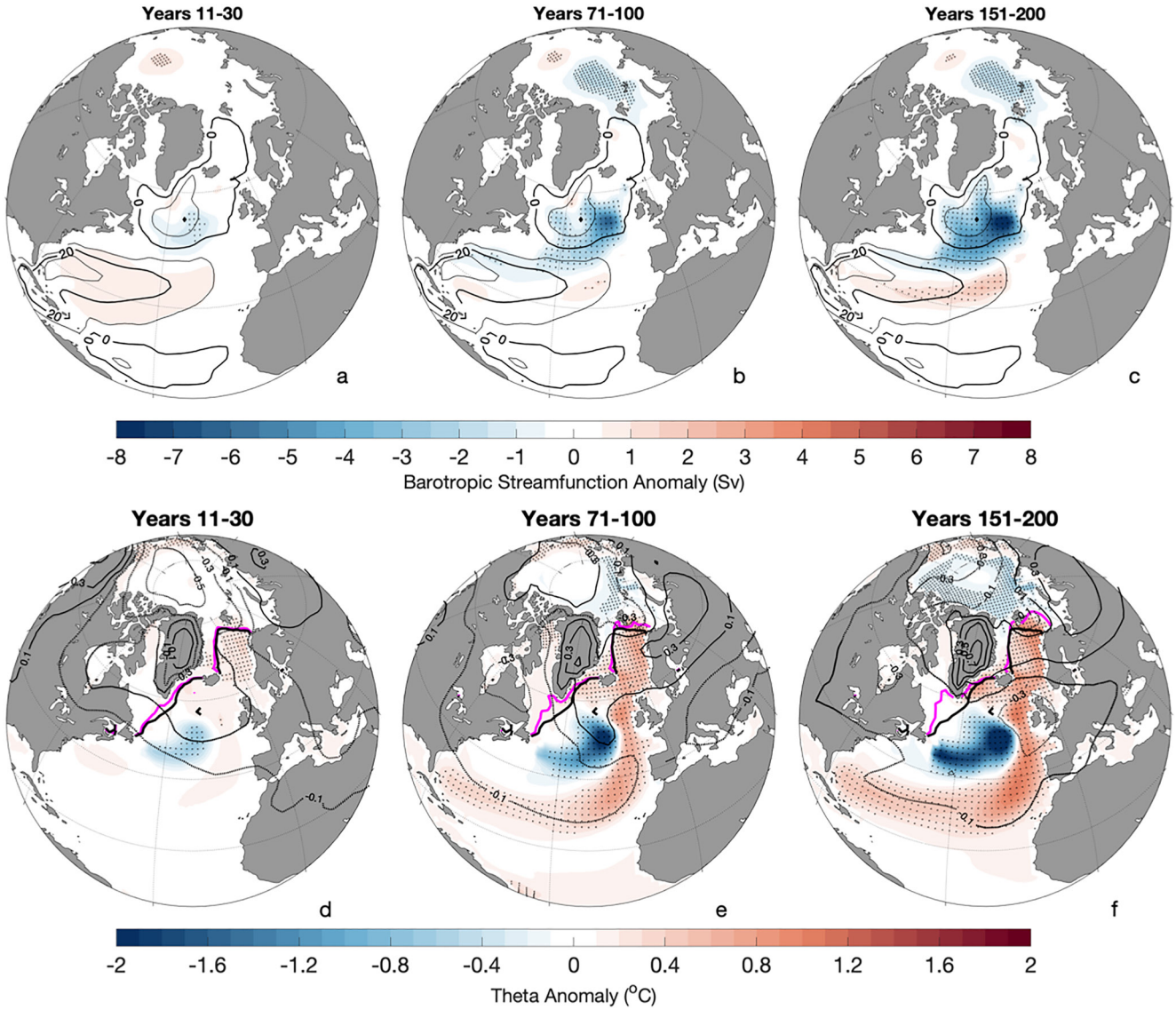

Figure 4. Anomalies in the (a–c) barotropic streamfunction and (d–f) ocean temperature averaged in the upper 300 m in the sea-ice perturbation experiment (color shading). Black contours in the top rows indicate mean barotropic streamfunction in the control experiment; positive values correspond to anticyclonic circulation. Contours of anomalous sea level pressure (SLP) are plotted analogous with theta (d–f), solid lines are positive and dashed lines are negative SLP anomalies. Hatching marks anomalies exceeding the 95% confidence level of the control. The 15% winter sea ice extent in the control (black) and perturbation (magenta) experiments is shown in bottom panels. Note the development of a pronounced "warming hole" in the bottom row, which is consistent with the intensification and southeastward expansion of the North Atlantic subpolar gyre in the top row (the black dot represents the minimum of the control for the subpolar North Atlantic).

(Figures S7b in Supporting Information S1) and is associated with a narrowing and intensifying of the northern hemisphere midlatitude westerlies and wind stress (Figures S7c and S7d in Supporting Information S1). The negative SLP_{NAO}-like pattern and anomalously reduced westerlies in the subpolar latitudes seen in ALB is thus consistent with the imposed SIA reduction.

The response in ocean circulation to reduced SIA and a negative NAO-like pattern induces a southeastern expansion of the SPG (Figures 4a–4c) and enhancement of the northward ocean circulation through the Iceland basin and toward the Arctic. In the Control experiment, winter SIA and SLP_{NAO} are positively correlated to the strength of the SPG (Figures S7e and S7f in Supporting Information S1), indicating that if the Arctic SIA and the NAO-like pattern are negative, there is a deepening of the negative barotropic streamfunction (BSF) in the subpolar North Atlantic. Moreover, zonal and meridional wind stress in the North Atlantic subpolar region is correlated with the SPG_{index} (Figures S7g–S7h in Supporting Information S1). The oceanic response to reduced

Arctic SIA occurs within the transient period, and by years 151–200 (Figure 4c) the SPG_{index} has intensified by ~4 Sv. Between 40° and 55°N, associated with the SPG deepening and expansion, a strong negative SST anomaly develops (Figures 4d–4f). This feature resembles the observed North Atlantic "warming hole" (NAWH), or the "cold blob," which is often attributed to a weakening AMOC (Drijfhout et al., 2012; Gervais et al., 2019; Liu et al., 2020). By years 151–200 the anomalous temperature in the NAWH core reached approximately −2°C in the upper 300 m (Figure 4f). This NAWH pattern is significantly correlated with variability in Arctic SIA, SLP_{NAO}, and surface wind stress (Figures S7i–S7l in Supporting Information S1). Moreover, at 0-lag, the AMOC and SPG are associated with distinct surface signals within the North Atlantic (Figures S8a–S8i in Supporting Information S1), showing the strong relationship with the NAWH region, but also theta, salinity, and potential density from the subpolar North Atlantic into the Nordic Seas.

Figure S8j in Supporting Information S1 shows that internal variability of the SLP_{NAO} pattern, AMOC at 55°N, and the SPG can drive theta variability in the NAWH region of the subpolar Atlantic, and that the NAWH can also influence the interannual-to-decadal variability of AMOC. In the case of the SPG, the largest correlations are when the SPG leads the NAWH variability, while the largest variability with AMOC is lagging that of the NAWH. In our experiments, AMOC is stabilizing in the long term (Figure 2, years 151–200) while NAWH continues to strengthen. Furthermore, using the CMIP5 ensemble mean relationship between the NAWH and the AMOC strength from Muir and Fedorov (2015, p. 0.3°C per 1 Sv) and Liu et al. (2020, 0.2°C per 1 Sv in CESM), the approximate −2°C NAWH response would require ~6–10 Sv of AMOC decline. Thus, it is likely that the NAWH could be driven by a combination of atmosphere and ocean changes (See Figures S7 and S8 in Supporting Information S1) rather than solely AMOC-driven, as discussed in Keil et al. (2020) and Hu and Fedorov (2020). Thus, in our experiment, the negative NAO-like pattern caused by the reduced sea ice cover could in part, drive the NAWH (Figures S6 and S7 in Supporting Information S1) through the anomalous SPG. As the NAWH strengthens and expands, density increases in the WSNA and decreased in the eastern subpolar North Atlantic, possibly further driving AMOC variability. This idea of multiple drivers of NAWH and in particular an atmospheric effect is consistent with the results of Li et al. (2022) and Hu and Fedorov (2020), even though in the latter study the wind changes are caused by remote teleconnections from the warming Indian Ocean.

Finally, the northward expansion of the negative BSF through the Iceland basin and into the Arctic (Figures 4a–4c) and a positive AMOC anomaly are associated with surface temperature, salinity, and density variability in the Barents Sea (Figures S4 and S8 in Supporting Information S1), consistent with the process of Atlantification described in Polyakov et al. (2017), Lind et al. (2018), Lique et al. (2018), and Årthun et al. (2019).

4. Discussions and Conclusions

In summary, we have conducted sensitivity experiments achieving a ~20% annual Arctic sea ice decline (~7% in winter and ~62% in summer) in the IPSL-CM5A2 via sea ice albedo reduction between years 150–200. The objective was to investigate the response of AMOC and the mechanisms driving the climate quasi-equilibrium response. The response of the AMOC to sea ice decline shows two distinct phases: first, a weakening of high-latitude overturning and deep (~1,000–2,500 m), high-density water formation, similar to what is found in previous experiments (i.e., Blackport and Kushner, 2016; Oudar et al., 2017; Sévellec et al., 2017; Liu et al., 2019, Li et al., 2021). This results in a shallower AMOC, declining at depth and compensating by less dense waters formation closer to the surface. Subsequently, the activation of DWF within the WSNA partly increased overturning of the upper, less dense (<27.6 kg m^{-3}) waters of the subtropical and subpolar regions to compensate for the decline within the Iceland basin. DWF from both regions are significantly correlated with the AMOC, where the Iceland Basin is related to the decline in deep overturning (~1,000–2,500 m) and the WSNA drives increased circulation within the upper-1000 m. The former change is largely driven by positive salinity and negative temperature anomalies, while the latter is driven by upper-ocean temperature increase. Together, the WSNA and Iceland Basin compensate by stabilizing the AMOC. The reduction of sea ice further results in a negative NAO-like pattern with a narrowing of the atmospheric westerlies and a southeastward expansion of the SPG. These adjustments further drive a NAWH, that persists and deepens despite weak changes in AMOC throughout the experiment. This suggests that the NAWH could be driven at least in part by changes in the atmospheric circulation.

The studies of Blackport and Kushner (2016) and Tomas et al. (2016) also showed an AMOC recovery at the end of their experiment of sea ice melting. However, our results contrast with another study based on a coupled GCM (CNRM-CM5, Oudar et al., 2017) using the same ocean model component and experiment setup, but having initially reduced (and thus more realistic) sea ice extent in the Labrador Sea region. In their experiment, the AMOC weakens by ∼−6 Sv, reaching 9–12 Sv in the approximate quasi-equilibrium (after 200 years of simulations); a similar strength to the mean state in IPSL-CM5A2 (∼11–13 Sv). By contrast, there is already deep convection in the Labrador and Irminger Seas at the beginning of the experiment with Oudar et al. (2017), so that the opening of the former plays a less important role. The different results between the two models underlines the possible sensitivity of the mechanism to the ocean mean state, where the IPSL-CM5A2 model exhibits a large initial sea ice bias compared to observations.

Our result is on the other hand consistent with Li et al. (2021), who conducted similar experiments using CESM1 with two different resolutions. The mean state of both models has no deep convection in the WSNA. However, the medium resolution model exhibits initial AMOC slowdown followed by recovery, which follows the activation of WSNA deep convection. The high-resolution model shows a sustained 30%–40% weakening of the AMOC and still no WSNA convection. Ocean resolution and bathymetry could thus also affect the results of sea ice perturbation experiments (Blackport and Screen, 2019; Screen et al., 2018). Differences with previous studies could also result from modeled AMOC stability and freshwater transports at 34°S. Mecking et al. (2017) showed that some models could be inherently monostable. For example, the IPSL-CM5A model has an M_{ov} at 34°S of −0.112, suggesting that AMOC is transporting salt into the Atlantic basin at this transect and is considered bi-stable, similar to what is thought for the observed regime. The concept of mono-/bi-stability could also play an important role in comparing these results. From Mecking et al. (2017), the shift of AMOC in a bi-stable system could result in AMOC stabilizing through anomalous freshwater transports into the Atlantic basin.

To conclude, direct comparison between various models is difficult, as the initial sea ice state and background climate could be pivotal in interpreting the impacts of Arctic sea ice decline in a warming climate. Across various modeling experiments, there are models that exhibit AMOC recovery and those that do not. This could be related to the stability of AMOC and freshwater transports (Li et al., 2021), and whether the strengthening of deep convection in the WSNA can compensate for the reduced deep-water formation in other regions, among other factors.

Acknowledgments
This research is supported by the ARCHANGE project of the "Make our planet great again" program (ANR-18-MPGA-0001, France) and by the Blue-Action project (European Union's Horizon 2020 research and innovation program, Grant 727852). Additional support is provided to AVF by NSF (OPP-1741841 and AGS-2053096). JM is supported by the EUCP project funded by the European Union's Horizon 2020 programme (grant agreement number 776613). EG is also supported by Centre National de la Recherche Scientifique (CNRS). AS acknowledges support from the Portuguese Foundation for Science and Technology through the FCT—project UIDB/50019/2020—IDL—Instituto Dom Luiz (IDL) and FCT—project JPIOCEANS/0001/2019 (ROADMAP: "The Role of ocean dynamics and Ocean–Atmosphere interactions in Driving cliMAte variations and future Projections of impact–relevant extreme events"). This work used the HPC resources of TGCC under the allocations 2019-A0070107403 provided by GENCI (Grand Equipement National de Calcul Intensif). This study benefited from the ESPRI (Ensemble de Services Pour la Recherche l'IPSL) computing and data centre (https://mesocentre.ipsl.fr) which is supported by CNRS, Sorbonne University, Ecole Polytechnique and CNES and through national and international grants. The authors would like to thank the two anonymous reviewers for their valuable comments and feedback.

Data Availability Statement

The datasets generated during the experiment are located on the TGCC machine Irene and several datasets to reproduce the results of the manuscript are published as Ferster et al. (2022) (https://doi.org/10.5281/zenodo.6572208).

References

Årthun, M., Eldevik, T., & Smedsrud, L. H. (2019). The role of Atlantic heat transport in future Arctic winter sea ice loss. *Journal of Climate*, *32*(11), 3327–3341. https://doi.org/10.1175/JCLI-D-18-0750.1

Blackport, R., & Kushner, P. J. (2016). The transient and equilibrium climate response to rapid summertime sea ice loss in CCSM4. *Journal of Climate*, *29*(2), 401–417. https://doi.org/10.1175/JCLI-D-15-0284.1

Blackport, R., & Screen, J. A. (2019). Influence of Arctic sea ice loss in autumn compared to that in winter on the atmospheric circulation. *Geophysical Research Letters*, *46*(4), 2213–2221. https://doi.org/10.1029/2018GL081469

Caian, M., Koenigk, T., Döscher, R., & Devasthale, A. (2018). An interannual link between Arctic sea-ice cover and the North Atlantic Oscillation. *Climate Dynamics*, *50*(1–2), 423–441. https://doi.org/10.1007/s00382-017-3618-9

Cohen, J., Screen, J. A., Furtado, J. C., Barlow, M., Whittleston, D., Francis, J., et al. (2014). Recent Arctic amplification and extreme mid-latitude weather. *Nature geoscience*, *7*(9), 627–637. https://doi.org/10.1038/NGEO2234

Cvijanovic, I., Santer, B. D., Bonfils, C., Lucas, D. D., Chiang, J. C., & Zimmerman, S. (2017). Future loss of Arctic sea-ice cover could drive a substantial decrease in California's rainfall. *Nature Communications*, *8*(1), 1–10. https://doi.org/10.1038/s41467-017-01907-4

Deser, C., Tomas, R. A., & Sun, L. (2015). The role of ocean-atmosphere coupling in the zonal-mean atmospheric response to Arctic sea ice loss. *Journal of Climate*, *28*(6), 2168–2186. https://doi.org/10.1175/JCLI-D-14-00325.1

Drijfhout, S., van Oldenborgh, G. J., & Cimatoribus, A. (2012). Is a decline of AMOC causing the warming hole above the North Atlantic in observed and modeled warming patterns? *Journal of Climate*, *25*(24), 8373–8379. https://doi.org/10.1175/JCLI-D-12-00490.1

Dufresne, J. L., Foujols, M. A., Denvil, S., Caubel, A., Marti, O., Aumont, O., et al. (2013). Climate change projections using the IPSL-CM5 Earth system model: From CMIP3 to CMIP5. *Climate Dynamics*, *40*(9), 2123–2165. https://doi.org/10.1007/s00382-012-1636-1

Ferster, B., Simon, A., Fedorov, A., Mignot, J., & Guilyardi, E. (2022). Climate response to ∼23% albedo reduction in IPSL-CM5A-LR (version v1). Retrieve from https://zenodo.org/record/6572208%23

García-Serrano, J., Frankignoul, C., Gastineau, G., & de la Cámara, A. (2015). On the predictability of the winter Euro-Atlantic climate: Lagged influence of autumn Arctic sea ice. *Journal of Climate*, *28*(13), 5195–5216. https://doi.org/10.1175/JCLI-D-14-00472.1

Gervais, M., Shaman, J., & Kushnir, Y. (2019). Impacts of the North Atlantic warming hole in future climate projections: Mean atmospheric circulation and the North Atlantic jet. *Journal of Climate*, *32*(10), 2673–2689. https://doi.org/10.1175/JCLI-D-18-0647.1

Heuzé, C. (2017). North Atlantic deep water formation and AMOC in CMIP5 models. *Ocean Science Discussions*, 1–22. https://doi.org/10.5194/os-2017-2

Hourdin, F., Foujols, M. A., Codron, F., Guemas, V., Dufresne, J. L., Bony, S., et al. (2013). Impact of the LMDZ atmospheric grid configuration on the climate and sensitivity of the IPSL-CM5A coupled model. *Climate Dynamics*, *40*(9–10), 2167–2192. https://doi.org/10.1007/s00382-012-1411-3

Hu, S., & Fedorov, A. V. (2020). Indian Ocean warming as a driver of the North Atlantic warming hole. *Nature Communications*, *11*(1), 4785. https://doi.org/10.1038/s41467-020-18522-5

Keil, P., Mauritsen, T., Jungclaus, J., Hedemann, C., Olonscheck, D., & Ghosh, R. (2020). Multiple drivers of the North Atlantic warming hole. *Nature Climate Change*, *10*(7), 667–671. https://doi.org/10.1038/s41558-020-0819-8

Kwon, Y., & Frankignoul, C. (2014). Mechanisms of multidecadal Atlantic meridional overturning circulation variability diagnosed in depth versus density space. *Journal of Climate*, *27*(24), 9359–9376. https://doi.org/10.1175/JCLI-D-14-00228.1

Li, H., Fedorov, A., & Liu, W. (2021). AMOC stability and diverging response to Arctic sea ice decline in two climate models. *Journal of Climate*, 1–47. https://doi.org/10.1175/JCLI-D-20-0572.1

Li, H., & Fedorov, A. V. (2021). Persistent freshening of the Arctic Ocean and changes in the North Atlantic salinity caused by Arctic sea ice decline. *Climate Dynamics*, *57*(11–12), 2995–3013. https://doi.org/10.1007/s00382-021-05850-5

Li, L., Lozier, M. S., & Li, F. (2022). Century-long cooling trend in subpolar North Atlantic forced by atmosphere: An alternative explanation. *Climate Dynamics*, *58*(9), 2249–2267. https://doi.org/10.1007/s00382-021-06003-4

Lind, S., Ingvaldsen, R. B., & Furevik, T. (2018). Arctic warming hotspot in the northern Barents Sea linked to declining sea-ice import. *Nature Climate Change*, *8*(7), 634–639. https://doi.org/10.1038/s41558-018-0205-y

Lique, C., Johnson, H. L., & Plancherel, Y. (2018). Emergence of deep convection in the Arctic Ocean under a warming climate. *Climate Dynamics*, *50*(9–10), 3833–3847. https://doi.org/10.1007/s00382-017-3849-9

Liu, W., & Fedorov, A. (2022). Interaction between Arctic sea ice and the Atlantic meridional overturning circulation in a warming climate. *Climate Dynamics*, *58*(5), 1811–1827. https://doi.org/10.1007/s00382-021-05993-5

Liu, W., Fedorov, A., & Sévellec, F. (2019). The mechanisms of the Atlantic meridional overturning circulation slowdown induced by Arctic sea ice decline. *Journal of Climate*, *32*(4), 977–996. https://doi.org/10.1175/JCLI-D-18-0231.1

Liu, W., & Fedorov, A. V. (2019). Global impacts of Arctic sea ice loss mediated by the Atlantic meridional overturning circulation. *Geophysical Research Letters*, *46*(2), 944–952. https://doi.org/10.1029/2018GL080602

Liu, W., Fedorov, A. V., Xie, S. P., & Hu, S. (2020). Climate impacts of a weakened Atlantic meridional overturning circulation in a warming climate. *Science Advances*, *6*(26), 1–9. https://doi.org/10.1126/sciadv.aaz4876

Madec, G., & the NEMO Team (2016). NEMO ocean engine. Note du Pôle de modélisation.

Mecking, J. V., Drijfhout, S. S., Jackson, L. C., & Andrews, M. B. (2017). The effect of model bias on Atlantic freshwater transport and implications for AMOC bi-stability. *Tellus A: Dynamic Meteorology and Oceanography*, *69*(1), 1299910. https://doi.org/10.1080/16000870.2017.1299910

Menary, M. B., Jackson, L. C., & Lozier, M. S. (2020). Reconciling the relationship between the AMOC and Labrador Sea in OSNAP observations and climate models. *Geophysical Research Letters*, *47*(18), e2020GL089793. https://doi.org/10.1029/2020GL089793

Meredith, M., Sommerkorn, M., Cassotta, S., Derksen, C., Ekaykin, A., Hollowed, A., et al. (2019). Polar regions. In H.-O. Pörtner, D. C. Roberts, V. Masson-Delmotte, (Eds.), *IPCC special report on the ocean and cryosphere in a changing climate*, *Water policy* (pp. 203–320). https://doi.org/10.1016/S1366-7017(01)00066-6

Muir, L. C., & Fedorov, A. V. (2015). How the AMOC affects ocean temperatures on decadal to centennial timescales: The North Atlantic versus an interhemispheric seesaw. *Climate Dynamics*, *45*(1), 151–160. https://doi.org/10.1007/s00382-014-2443-7

Notz, D., & Community, S. (2020). Arctic sea ice in CMIP6. *Geophysical Research Letters*, *47*(10), 1–11. https://doi.org/10.1029/2019GL086749

Ortega, P., Robson, J. I., Menary, M., Sutton, R. T., Blaker, A., Germe, A., et al. (2021). Labrador Sea subsurface density as a precursor of multidecadal variability in the north Atlantic: A multi-model study. *Earth System Dynamics*, *12*(2), 419–438. https://doi.org/10.5194/esd-12-419-2021

Oudar, T., Sanchez-Gomez, E., Chauvin, F., Cattiaux, J., Terray, L., & Cassou, C. (2017). Respective roles of direct GHG radiative forcing and induced Arctic sea ice loss on the Northern Hemisphere atmospheric circulation. *Climate Dynamics*, *49*(11–12), 3693–3713. https://doi.org/10.1007/s00382-017-3541-0

Overland, J. E., & Wang, M. (2013). When will the summer Arctic be nearly sea ice free? *Geophysical Research Letters*, *40*(10), 2097–2101. https://doi.org/10.1002/grl.50316

Polyakov, I. V., Pnyushkov, A. V., Alkire, M. B., Ashik, I. M., Baumann, T. M., Carmack, E. C., et al. (2017). Greater role for Atlantic inflows on sea-ice loss in the Eurasian basin of the Arctic ocean.

Screen, J. A., Deser, C., Smith, D. M., Zhang, X., Blackport, R., Kushner, P. J., et al. (2018). Consistency and discrepancy in the atmospheric response to Arctic sea-ice loss across climate models. *Nature Geoscience*, *11*(3), 155–163. https://doi.org/10.1038/s41561-018-0059-y

Sepulchre, P., Caubel, A., Ladant, J. B., Bopp, L., Boucher, O., Braconnot, P., et al. (2020). IPSL-CM5A2 - an Earth system model designed for multi-millennial climate simulations. *Geoscientific Model Development*, *13*(7), 3011–3053. https://doi.org/10.5194/gmd-13-3011-2020

Sévellec, F., Fedorov, A. V., & Liu, W. (2017). Arctic sea-ice decline weakens the Atlantic meridional overturning circulation. *Nature Climate Change*, *7*(8), 604–610. https://doi.org/10.1038/NCLIMATE3353

Simon, A., Frankignoul, C., Gastineau, G., & Kwon, Y. O. (2020). An observational estimate of the direct response of the cold-season atmospheric circulation to the arctic sea ice loss. *Journal of Climate*, *33*(9), 3863–3882. https://doi.org/10.1175/JCLI-D-19-0687.1

Simon, A., Gastineau, G., Frankignoul, C., Rousset, C., & Codron, F. (2021). Transient climate response to Arctic sea ice loss with two ice-constraining methods. *Journal of Climate*, *34*(9), 3295–3310. https://doi.org/10.1175/jcli-d-20-0288.1

Smith, D. M., Eade, R., Andrews, M. B., Ayres, H., Clark, A., Chripko, S., et al. (2022). Robust but weak winter atmospheric circulation response to future Arctic sea ice loss. *Nature Communications*, *13*(1), 727. https://doi.org/10.1038/s41467-022-28283-y

Speer, K., & Tziperman, E. (1992). Rates of water mass formation in the North Atlantic ocean. *Journal of Physical Oceanography*, *22*(1), 93–104. https://doi.org/10.1175/1520-0485(1992)022%3c0093:ROWMFI%3e2.0.CO;2

Sun, L., Alexander, M., & Deser, C. (2018). Evolution of the global coupled climate response to Arctic sea ice loss during 1990-2090 and its contribution to climate change. *Journal of Climate*, *31*(19), 7823–7843. https://doi.org/10.1175/JCLI-D-18-0134.1

Suo, L., Gao, Y., Guo, D., & Bethke, I. (2017). Sea-ice free Arctic contributes to the projected warming minimum in the North Atlantic. *Environmental Research Letters*, *12*(7), 074004. https://doi.org/10.1088/1748-9326/aa6a5e

Tomas, R. A., Deser, C., & Sun, L. (2016). The role of ocean heat transport in the global climate response to projected arctic sea ice loss. *Journal of Climate*, *29*(19), 6841–6859. https://doi.org/10.1175/JCLI-D-15-0651.1

Walin, G. (1982). On the relation between sea-surface heat flow and thermal circulation in the ocean. *Tellus*, *34*(2), 187–195. https://doi.org/10.3402/tellusa.v34i2.10801

Zhang, R. (2015). Mechanisms for low-frequency variability of summer Arctic sea ice extent. *Proceedings of the National Academy of Sciences*, *112*(15), 4570–4575. https://doi.org/10.1073/pnas.1422296112

References From the Supporting Information

Giles, K. A., Laxon, S. W., Ridout, A. L., Wingham, D. J., & Bacon, S. (2012). Western Arctic Ocean freshwater storage increased by wind-driven spin-up of the Beaufort Gyre. *Nature Geoscience*, *5*(3), 194–197. https://doi.org/10.1038/ngeo1379

Jackett, D. R., & McDougall, T. J. (1997). A neutral density variable for the world's oceans. *Journal of Physical Oceanography*, *27*(2), 237–263. https://doi.org/10.1175/1520-0485(1997)027<0237:ANDVFT>2.0.CO;2

Meier, W. N., Fetterer, F., Windnagel, A. K., & Stewart, J. S. (2021). *NOAA/NSIDC climate data record of passive microwave sea ice concentration, version 4.1*. NSIDC: National Snow and Ice Data Center. https://doi.org/10.7265/efmz-2t65

Seidenglanz, A., Athanasiadis, P., Ruggieri, P., Cvijanovic, I., Li, C., & Gualdi, S. (2021). Pacific circulation response to eastern Arctic sea ice reduction in seasonal forecast simulations. *Climate Dynamics*, *57*(9), 2687–2700. https://doi.org/10.1007/s00382-021-05830-9